Progress In Electromagnetics Research, Vol. 125, 527–542, 2012

A NOVEL IMAGE FORMATION ALGORITHM FOR HIGH-RESOLUTION WIDE-SWATH SPACEBORNE SAR USING COMPRESSED SENSING ON AZIMUTH DISPLACEMENT PHASE CENTER ANTENNA

J. Chen*, J. H. Gao, Y. Q. Zhu, W. Yang, and P. B. Wang

School of Electronics and Information Engineering, Beihang University, Beijing 100191, China

Abstract—High-resolution wide-swath (HRWS) imaging with spaceborne synthetic aperture radar (SAR) can be achieved by using azimuth displacement phase center antenna (DPCA) technique. However, it will consequently leads to extremely high data rate on satellite downlink system. A novel sparse sampling scheme based on compressed sensing (CS) theory for azimuth DPCA SAR was proposed, by which only a small proportion of radar echoes are utilized for imaging to reduce data rate. The corresponding image formation algorithm for the proposed scheme was presented in the paper. The SAR echo signal of each channel can be reconstructed with high probability by using orthogonal matching pursuit (OMP) algorithm in Doppler frequency domain. The reconstructed echo signals of each channel are jointly processed by means of spectrum reconstructing filter for compensating Doppler spectrum aliasing resulting from non-uniform sampling in azimuth direction. The high quality SAR image can be obtained by using chirp scaling algorithm. The effectiveness of the proposed approach was validated by computer simulations using both point targets and distributed targets.

1. INTRODUCTION

The increasing demands on high-resolution wide-swath (HRWS) spaceborne synthetic aperture radar (SAR) are arising among several applications, e.g., ocean surveillance, disaster monitoring, etc. [1–5]. High-resolution and wide-swath are contradictions with the conventional single-channel spaceborne SAR systems [6–9]. But, it can

Received 11 December 2011, Accepted 27 February 2012, Scheduled 7 March 2012
* Corresponding author: Jie Chen (chenjie@buaa.edu.cn).

be mitigated by using azimuth Displacement Phase Center Antenna (DPCA) technique, if azimuth spectrum aliasing in case of non-DPCA condition is accurately compensated [6–8]. DPCA has been successfully applied in the advanced spaceborne SAR systems, e.g., RADARSAT-II and TerraSAR-X. However, the multi-channel receivers in DPCA lead to huge data volume, which challenges both on-board storage and downlink subsystem of the SAR satellite.

Recently, Donoho [10] proposed a new theory of compressed sensing (CS). The basic principle of CS is to reduce the number of measurements lower than the limitation imposed by Nyquist theory, if it is known that a signal has a sparse representation in some transform domain [10–13]. Considering SAR image is a map of the spatial distribution of the reflectivity of stationary targets, many SAR images are sparse or compressible under a certain basis. Some researchers applied CS theory on imaging radar, including SAR and ISAR [14–19]. Baraniuk and Steeghs [17] proposed a novel compressive radar receiver based on CS to reduce A/D converter rate at radar receiver. The signals were reconstructed by means of orthogonal matching pursuit (OMP) greedy algorithm [20]. Moreover, Varshney et al. [18] studied a reduced set of randomly samples to reduce the amount of data samples collected at the radar receiver, and employed the regularized OMP (ROMP) to reconstruct SAR image [18]. Patel et al. [19] investigated the sparse signal representation from complete dictionaries [19]. Most recent studies on implementation of CS based SAR techniques assumed the radar targets in the scene are sparse. However, the approaches discussed in above literatures [14–19] only concentrated on the application of CS theory for conventional single-channel SAR systems, which cannot be directly applied to azimuth DPCA SAR systems without modification on azimuth spectrum aliasing compensation.

In order to solve such problem, we developed a new approach for spaceborne DPCA SAR based on CS theory in this paper. The compressibility of the echo signal in azimuth time domain was investigated, to make the echo signal sparse in Fourier domain via sparse processing. Then the random Gaussian matrix was utilized as sampling matrix. A small proportion of SAR echoes are randomly collected at sub-Nyquist-rate in azimuth direction among the multi-channel receivers in DPCA, which significantly reduces downlink data rate. Then, the original fully-sampled signal can be reconstructed with OMP algorithm [20] in Doppler frequency domain, and the Doppler spectrum can be reconstructed by means of conventional reconstruction filter. The traditional chirp scaling image formation algorithm was employed in azimuth direction without losing main information of

sparse targets (e.g., ships in the ocean).

The remainder of this paper is organized as follows. In Section 2, the basic principle of CS was introduced. In Section 3, the azimuth DPCA SAR is briefly reviewed. In Section 4, a novel sparse sampling scheme based on CS theory for azimuth DPCA SAR, namely CS-HRWS SAR, is proposed. The corresponding image formation algorithm for the proposed CS-HRWS SAR scheme is presented in Section 5. In order to validate the proposed approach, simulation experiments with both point targets and distributed targets were carried out in Section 6. Finally, the conclusions and discussions are presented in Section 7.

2. COMPRESSED SENSING PRINCIPLE

Compressed sensing (CS) is a newly developed theory which enables the reconstruction of sparse signal by projecting high dimensional signal on a lower dimensional space [10]. The signal can be recovered with high probability using CS, if the signal is compressible or sparse, which means only small number of samples are required to reconstruct original signal within certain error bound. Sparsity can be defined as ratio of non-zero elements to total number of elements in a signal in time or spatial domain. In a transform domain, it is defined as ratio of number of non-zero coefficients to total number of coefficients required to reconstruct the original signal. Higher sparsity level will lead to less number of samples used for reconstructing the original signal. According to CS theory, the number of measurements can be much smaller than the number of Nyquist-rate samples [12].

Consider a finite discrete-time signal vector $s \in R^{\mathbf{N}}$ is K-sparse under a certain orthogonal basis $\mathbf{\Psi} \in \mathbf{C}^{N \times N}$, and the sparse signal can be expressed as:

$$\mathbf{x} = \mathbf{\Psi s} \tag{1}$$

where $\|\mathbf{x}\|_0 = K \ll N$, $\|\|_0$ denotes l_0 norm. Vector $\mathbf{x}$ is sparse representation of original signal vector $\mathbf{s}$ in $\mathbf{\Psi}$ domain. In fact, under CS theory, final observation is not in $\mathbf{\Psi}$ domain, but is a projection of $\mathbf{s}$ onto a random $M \times N$ measurement matrix $\mathbf{\Phi} = [\phi_1, \phi_2, \ldots, \phi_N]$, with $M < N$. It makes sense that only M samples of signal $\mathbf{s}$ need to be measured instead of N samples. The measurements signal $\mathbf{y} \in R^M$ is described as:

$$\mathbf{y} = \mathbf{\Phi s} = \mathbf{\Phi \Psi^H x} = \mathbf{\Theta x} \tag{2}$$

where $\mathbf{\Theta} = \mathbf{\Phi \Psi}$ is a $M \times N$ matrix and $\mathbf{\Psi^H}$ is transpose matrix of $\mathbf{\Psi}$. The inverse problem of solving Equation (2) is an ill-posed problem, and the original signal $\mathbf{s}$ cannot be directly measured by M observation

values. However, it is possible to recover the sparse signal via CS when measurement matrix $\mathbf{\Phi}$ and vector $\mathbf{x}$ satisfies the restricted isometry property (RIP), which requires that:

$$1 - \delta_k \leq \frac{\|\mathbf{\Theta x}\|_2^2}{\|\mathbf{x}\|_2^2} \leq 1 - \delta_k \tag{3}$$

where $\delta_k \in (0, 1)$. The RIP is closely related to an incoherency property. It is proved that the random matrix performs well [10]. If the number of measurements $M \geq K \log(N/K)$, the K-sparse signal $\mathbf{s}$ can be exactly reconstructed with high probability [12].

When $\mathbf{\Phi}$ satisfies RIP, the reconstruction is achieved by estimation via a convex optimization problem based on l_1 norm:

$$\min \|x\|_1 \ \ s.t.\ y = \mathbf{\Theta} x \tag{4}$$

Current reconstruction method includes greedy algorithms such as basic pursuit (BP), orthogonal matching pursuit (OMP) and regularized orthogonal matching pursuit (ROMP), etc. [18].

3. SPACEBORNE AZIMUTH DPCA SAR

Spaceborne azimuth DPCA technique is an effective approach for implementation of high-resolution wide-swath SAR imaging. Fig. 1

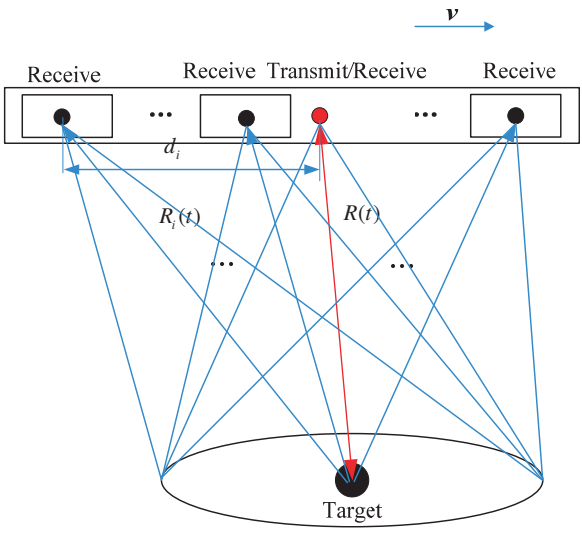

Figure 1. Azimuth multi-channel SAR geometry.

illustrates the geometry of spaceborne azimuth DPCA SAR, where the whole antenna transmits radar pulses and L sub-aperture antennas simultaneously receive the scattered echo signals from the illuminated targets. For the i-th receiver separated by distance d_i from the antenna phase center, the echo signal can be written as:

$$\mathbf{S}^{(i)}(t,\tau) = \sigma W_a(t) \exp\left\{-j\frac{2\pi}{\lambda}(R(t)+R_i(t))\right\}$$
$$\exp\left\{-j\pi b\left[\tau - \frac{R(t)+R_i(t)}{c}\right]^2\right\} = \sigma W_a(t) h_{si}(t) h_{si}(\tau), \quad i=1,2,\ldots,L \quad (5)$$

where σ is backscatter coefficient, $W_a(t)$ is antenna pattern, t is azimuth time, τ is range time, $h_{si}(t)$ and $h_{si}(\tau)$ denote azimuth and range impulse response function, respectively; λ denotes wavelength, $R(t)$ denotes the slant range from the transmitter to the scatter, $R_i(t)$ denotes the slant range of the i-th receiver.

The echo data sample received at the i-th receiver can be written in digital signal form as:

$$\mathbf{S}^{(i)}(m,n) = \sigma W_a(m/f_p) h_{si}(m/f_p) h_{si}(n/f_s), \ 1 \le m \le N_a, \ 1 \le n \le N_r \quad (6)$$

where $t = (m - N_a/2)/f_p$, $\tau = (n - N_r/2)/f_s$, $m = 1, 2, \ldots, N_a$, $n = 1, 2, \ldots, N_r$.

For simplification, $\mathbf{S}^{(i)}(m, n)$ can be rewritten in array format, which is given by:

$$\mathbf{S}^{(i)}_{N_a \times N_r} = \begin{bmatrix} s^{(i)}_{11} & s^{(i)}_{12} & \cdots & s^{(i)}_{1N_r} \\ s^{(i)}_{21} & s^{(i)}_{22} & \cdots & s^{(i)}_{2N_r} \\ \vdots & \vdots & \vdots & \vdots \\ s^{(i)}_{N_a1} & s^{(i)}_{N_a2} & \cdots & s^{(i)}_{N_aN_r} \end{bmatrix} = \left[\mathbf{S}^{(i)}_1 \ \mathbf{S}^{(i)}_2 \ \cdots \ \mathbf{S}^{(i)}_{N_r}\right], \quad i=1,2,\ldots,L \quad (7)$$

where $\mathbf{S}^{(i)}_{N_a \times N_r}$ denotes the echo data array received at the i-th receiver with size of $N_a \times N_r$, $\mathbf{S}^{(i)}_n = [s^{(i)}_{1n}, s^{(i)}_{2n}, \ldots s^{(i)}_{N_an}]^T$ denotes azimuth echo signal vector with size of $N_a \times 1$ at a given range cell.

For each transmitted pulse, the multi-channel receivers in DPCA simultaneously receive L records of radar echoes. Therefore, the radar can operate at lower pulse repetition frequency (PRF), which is one over L of the required PRF, without increasing azimuth ambiguities. The echo signals by multiple receivers can be combined into one data array with the required PRF. Such processing is called reconstruction filter, which allows for unambiguous reconstruction of original signal from aliased spectra with the L representations [6].

4. SPARSE SAMPLING SCHEME FOR CS-HRWS SAR

A novel sparse sampling scheme for azimuth DPCA SAR based on CS theory is proposed in this section, to implement lower data rate for spaceborne CS-HRWS SAR system.

4.1. Azimuth Time Domain Sparse Processing

An important prerequisite of CS sparse reconstruction is that the signal must be sparse or compressible in certain representations [21, 22]. However, the echo data are not sparse in azimuth direction without any disposing. To enhance the sparsity of original signal in azimuth direction, the pre-processing of coarse focusing should be employed in azimuth direction, by means of multiplying the original signal with a reference phase term in each column, shown as follows:

$$\mathbf{P}^{(i)} = \left[\mathbf{P}_1^{(i)}\, \mathbf{P}_2^{(i)}\, \ldots\, \mathbf{P}_{N_r}^{(i)}\right], \quad i = 1, 2, \ldots, L \tag{8}$$

and

$$\mathbf{P}_n^{(i)} = \mathbf{S}_n^{(i)} \cdot \mathbf{h}_{si}, \quad n = 1, 2, \ldots, N_r,$$

where $\mathbf{P}_n^{(i)}$ $(n = 1, 2, \ldots, N_r)$ is column vector of matrix $\mathbf{P}^{(i)}$, which is the signal after spare processing in azimuth direction of the i-th channel. $\mathbf{h}_{si} = [\eta_1, \eta_2, \ldots, \eta_{Na}]^T$ denotes the column vector of the reference phase term, where $\eta_m = \exp\{j\frac{2\pi}{\lambda}[R(m/f_p) + R_i(m/f_p)]\}$, $m = 1, 2, \ldots, N_a$.

Most of elements are close to the same value after sparse processed in azimuth time domain, and the processed signal of each channel can be represented with the small number of significant coefficients under Fourier basis, i.e., the signal becomes sparse in azimuth frequency domain.

4.2. Azimuth Frequency Domain Sparse Representation

The processed azimuth echo signal of each channel is then projected into azimuth frequency domain. Fourier basis was chosen as the transform matrix $\mathbf{\Psi}$, the definition of $\mathbf{\Psi}$ is given by:

$$\mathbf{\Psi} = \frac{1}{\sqrt{N_a}} \begin{bmatrix} 1 & 1 & \ldots & 1 \\ 1 & \exp\left\{\frac{-j2\pi}{N_a}\right\} & \ldots & \exp\left\{\frac{-j2(N_a-1)\pi}{N_a}\right\} \\ \vdots & \vdots & \ldots & \vdots \\ 1 & \exp\left\{\frac{-j2(N_a-1)\pi}{N_a}\right\} & \ldots & \exp\left\{\frac{-j2(N_a-1)^2\pi}{N_a}\right\} \end{bmatrix} \tag{9}$$

where N_a is the length of echo signal in azimuth direction, $\mathbf{\Psi}$ satisfies orthogonality $\mathbf{\Psi} = \mathbf{\Psi}^H$. The sparse signal of each channel in $\mathbf{\Psi}$ domain can be written as:

$$\begin{aligned}\mathbf{P}^{(i)} &= \mathbf{\Psi}^H \mathbf{X}^{(i)} = \mathbf{\Psi}^H \left[\mathbf{X}_1^{(i)}\, \mathbf{X}_2^{(i)}\, \ldots\, \mathbf{X}_{N_r}^{(i)}\right] \\ &= \left[\mathbf{P}_1^{(i)}\, \mathbf{P}_2^{(i)}\, \ldots\, \mathbf{P}_{N_r}^{(i)}\right], \quad i = 1, 2, \ldots, L \end{aligned} \tag{10}$$

where $\mathbf{\Psi}^H$ denotes transposed matrix of $\mathbf{\Psi}$, $\mathbf{X}_n^{(i)}$ $(n = 1, 2, \ldots, N_r)$ is sparse representation of $\mathbf{P}^{(i)}$ in $\mathbf{\Psi}$ domain with size $N_a \times 1$, and has K strongest nonzero coefficients with $K \ll N_a$ where K denotes the number of targets in azimuth direction.

4.3. Sparse Sampling in Azimuth Time Domain

In order to use CS, a linear sampling model of SAR is required. Here, a random Gaussian matrix was selected as the sampling matrix since it would satisfy the RIP with high probability [12]. The linear measurement result can be written as:

$$\mathbf{Y}^{(i)} = \mathbf{\Phi}\mathbf{P}^{(i)} = \mathbf{\Phi}\left\{\mathrm{Re}\left(\mathbf{P}^{(i)}\right),\ \mathrm{Im}\left(\mathbf{P}^{(i)}\right)\right\}, \quad i = 1, 2, \ldots, L \tag{11}$$

where $\mathrm{Re}\left(\mathbf{P}^{(i)}\right)$ and $\mathrm{Im}\left(\mathbf{P}^{(i)}\right)$ are the real and imaginary part of $\mathbf{P}^{(i)}$ respectively. $\mathbf{Y}^{(i)}$ is linear measurement result with size $M \times 1$. Putting (10) into (11) we can derive:

$$\mathbf{Y}^{(i)} = \mathbf{\Phi}\mathbf{P}^{(i)} = \mathbf{\Phi}\mathbf{\Psi}^H\mathbf{X}^{(i)} = \mathbf{\Theta}\left\{\mathrm{Re}\left(\mathbf{X}^{(i)}\right), \mathrm{Im}\left(\mathbf{X}^{(i)}\right)\right\}, \quad i = 1 \ldots L \tag{12}$$

where $\mathrm{Re}\left(\mathbf{X}^{(i)}\right)$ and $\mathrm{Im}\left(\mathbf{X}^{(i)}\right)$ are the real and imaginary part of $\mathbf{X}^{(i)}$ respectively.

5. SPACEBORNE CS-HRWS SAR IMAGE FORMATION

5.1. Sparse Reconstruction in Azimuth Frequency Domain

According to Equations (6)–(12) the frame of CS is constructed, and the reconstruction is achieved by means of estimation through a convex optimization problem based on l_1 norm, shown as follows:

$$\min \left\|\widehat{\mathbf{X}}_n^{(i)}\right\|_1 \text{ s.t. } \mathbf{Y}^{(i)} = \mathbf{\Theta}\widehat{\mathbf{X}}^{(i)}, \quad i = 1, 2, \ldots, L \tag{13}$$

OMP algorithm is adopted to solve Equation (13) and then the sparse signal of $\widehat{\mathbf{X}}_n^{(i)}$ $(n = 1, 2, \ldots, N_r)$ is derived from frequency domain. The OMP algorithm built up a solution element by element which based on the simple fact that the element was strongly correlated with signal's residual.

5.2. Phase Compensation in Azimuth Frequency Domain

In order to compensate for the eliminated phase term in (8), the reconstructed signal $\widehat{\mathbf{X}}_n^{(i)}$ ($n = 1, 2, \ldots, N_r$) should be convolved with reference function $\mathbf{h}_{si}^*$ in frequency domain. The recovered original signal can be given as:

$$\widehat{\mathbf{P}}_n^{(i)} = \widehat{\mathbf{X}}_n^{(i)} \otimes F\left(\mathbf{h}_{si}^*\right), \quad i = 1, 2, \ldots, L, \quad n = 1, 2, \ldots, N_r \tag{14}$$

where $\mathbf{h}_{si}^*$ denotes conjugate of $\mathbf{h}_{si}$, $\widehat{\mathbf{P}}_n^{(i)}$ is the recovered signal and $F(\cdot)$ denotes Fourier transform.

5.3. Spectrum Reconstruction in Azimuth Frequency Domain

The spectrum reconstruction algorithm is based on the theory of combining L independent representations of each echo signal; each channel samples the echo with $1/L$ the Nyquist frequency [6]. This allows the unambiguous reconstruction of the original signal from the aliased spectra of the L representative multiple radar echoes. The echo signals collected at different spatial positions are jointly processed through a filter which is shifted by integer multiples of the PRF in the frequency domain shown as follows:

$$\widehat{\mathbf{S}}_n = \widehat{\mathbf{P}}_n^{(i)} \cdot \mathbf{H}(f), \quad n = 1, 2, \ldots, N_r, \quad i = 1, 2, \ldots, L \tag{15}$$

where

$$\mathbf{H}(f) = \begin{bmatrix} \exp\left\{-j\frac{d_1}{2v}2\pi f_a\right\} & \exp\left\{-j\frac{d_2}{2v}2\pi f_a\right\} & \ldots & \exp\left\{-j\frac{d_L}{2v}2\pi f_a\right\} \\ \exp\left\{-j\frac{d_1}{2v}(2\pi f_a + f_p)\right\} & \exp\left\{-j\frac{d_2}{2v}(2\pi f_a + f_p)\right\} & \ldots & \exp\left\{-j\frac{d_L}{2v}(2\pi f_a + f_p)\right\} \\ \vdots & \vdots & & \vdots \\ \exp\left\{-j\frac{d_1}{2v}\left[2\pi f_a + (L-1)f_p\right]\right\} & \exp\left\{-j\frac{d_2}{2v}\left[2\pi f_a + (L-1)f_p\right]\right\} & \ldots & \exp\left\{-j\frac{d_L}{2v}\left[2\pi f_a + (L-1)f_p\right]\right\} \end{bmatrix}^{-1},$$

By using the reconstruct filter, the spectrum of all the azimuth signals is reconstructed without aliasing.

5.4. SAR Image Formation Processing

The chirp scaling imaging algorithm has matured. Theoretically, it is possible to adopt the multi-channel SAR signal model for a complete reconstruction of the scene reflectivity. Due to the reconstructed azimuth signal is already in range Doppler domain, the main steps of the chirp scaling algorithm includes: applying chirp scaling; Range FFT which transform the reconstructed signal into two-dimensional frequency domain; a phase multiply applies range compression; Range IFFT which transform the signal back to the range Doppler domain; a phase multiply is performed to apply azimuth compression with a range-varying matched filter; the final step is an azimuth IFFT to transform the compressed data back to two-dimensional time domain, which is the SAR image domain. The whole processing flowchart is shown in Fig. 2.

6. SIMULATION AND DISCUSSIONS

To evaluate the validity of the proposed CS-HRWS SAR imaging algorithm, the computer simulation experiments were carried out on nine point targets array with constant scattering coefficients. The parameters for spaceborne CS-HRWS SAR are listed in Table 1.

According to the given parameters, the SAR system has single transmit phase center and three receive phase centers. The PRF of

Table 1. Simulation parameters.

Parameters	Values
Subaperture Number N	3
Wavelength λ (m)	0.03
Altitude H (km)	495
Slant Range R (km)	700
Antenna Length L (m)	15
Band width B_r (MHz)	120
Sampling Rate f_s (MHz)	144
Sparse Sampling Rate M	1/8
Subaperture Length d (m)	5
Pulse Width T_r (μs)	20
Satellite Velocity v (m/s)	7500
Pulse Repeat Frequency (PRF) f_p (Hz)	1200
Incidence Angle θ (deg)	45

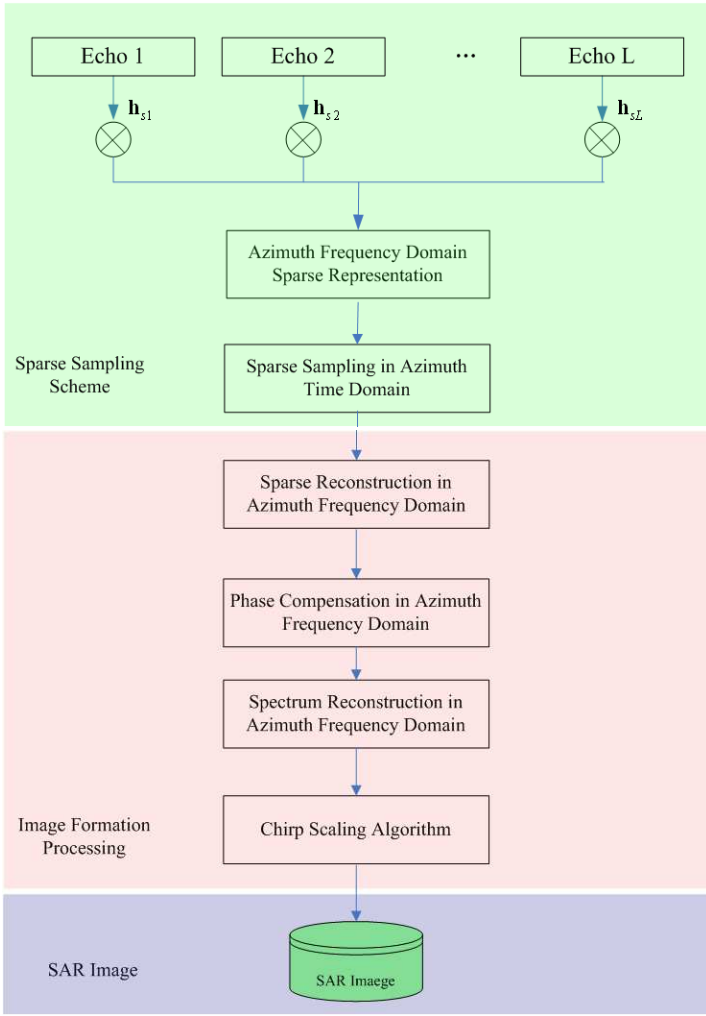

Figure 2. Flowchart of spaceborne CS-HRWS SAR processing.

the spaceborne CS-HRWS SAR is 1200 Hz, with the corresponding swath-width is 75 km. The reconstructed Doppler bandwidth is near 3000 Hz, with corresponding azimuth resolution of 2.5 m. The original data rate of the spaceborne HRWS SAR system is 1451 Mbps, which is difficult for satellite downlink subsystem.

The radar echoes are simulated based on Equation (5). And, the raw echo signals were sparsely processed according to Equation (8) in the first step, and then the processed signals are projected into Fourier

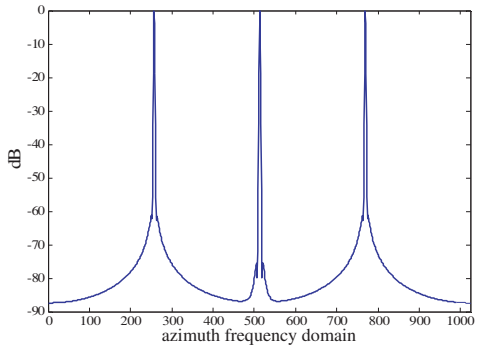

Figure 3. Sparse processing in azimuth time domain.

Figure 4. Imaging result of the proposed CS-HRWS SAR with 12.5% sampling.

Figure 5. Imaging result of conventional DPCA SAR with full samples of raw data.

basis (see Fig. 3). Fig. 3 illustrates that the echo signal after sparse processing shows distinct sparsity in azimuth frequency domain, which indicates the possibility of using CS theory.

Only 12.5% received echo records were randomly selected in azimuth direction among the receiving channels. The data rate was reduced to 181 Mbps with the novel CS-HRWS scheme.

The multi-channel raw data can be reconstructed with CS theory if the targets are sparse in certain domain. The reconstructed SAR images of the point targets using the proposed method and conventional method with full samples are shown in Figs. 4 and 5. Comparing Fig. 4 with Fig. 5, it shows that the proposed CS-HRWS SAR with 12.5% sampling rate can generate the nearly same image quality as the conventional DPCA SAR.

To further validate the proposed method, the imaging results shown in Figs. 4 and 5 are quantitatively evaluated by means of the spatial resolution, and Peak Side Lobe Ratio (PSLR) as well as Integrated Side Lobe Ratio (ISLR) [23]. The resolution, PSLR and the ISLR of the nine point targets simulation with the proposed CS-HRWS SAR and conventional DPCA SAR are listed in Tables 2 and 3, respectively.

Table 2. Evaluating results of the proposed CS-HRWS SAR with 12.5% sampling rate.

Points	Azimuth			Slant Range		
	ρ_a	PSLR	ISLR	ρ_{gr}	PSLR	ISLR
1	2.714	−26.026	−21.507	1.379	−25.946	−20.813
2	2.710	−26.027	−21.423	1.381	−26.473	−20.833
3	2.710	−26.017	−21.440	1.379	−25.940	−20.817
4	2.714	−26.168	−21.488	1.381	−25.972	−20.836
5	2.710	−26.138	−21.421	1.381	−26.447	−20.835
6	2.714	−26.172	−21.492	1.381	−25.931	−20.826
7	2.710	−25.956	−21.445	1.381	−25.952	−20.831
8	2.710	−25.982	−21.444	1.381	−26.474	−20.843
9	2.714	−26.013	−21.496	1.379	−25.941	−20.817

Table 3. Evaluating results of conventional DPCA SAR with full samples of raw data.

Points	Azimuth			Slant Range		
	ρ_a	PSLR	ISLR	ρ_{gr}	PSLR	ISLR
1	2.710	−25.958	−21.390	1.381	−25.975	−20.831
2	2.710	−25.972	−21.396	1.381	−26.506	−20.849
3	2.710	−25.981	−21.396	1.381	−25.975	−20.828
4	2.706	−26.152	−21.409	1.381	−25.975	−20.831
5	2.706	−26.180	−21.415	1.381	−26.506	−20.849
6	2.706	−26.203	−21.416	1.381	−25.975	−20.828
7	2.706	−25.902	−21.388	1.381	−25.975	−20.831
8	2.706	−25.931	−21.394	1.381	−26.506	−20.849
9	2.706	−25.954	−21.396	1.381	−25.975	−20.823

Figure 6. Original TerraSAR image as distributed targets for echo simulation.

Figure 7. Imaging result of conventional DPCA SAR full samples of raw data.

(a)

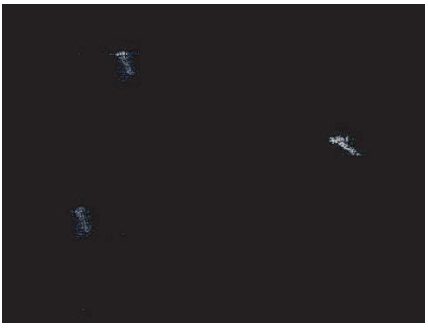

(b)

Figure 8. Imaging result of the proposed spaceborne CS-HRWS SAR with different azimuth sampling rate. (a) With 50% samples, (b) with 25% samples.

Comparing the image quality evolution results listed in Tables 2 and 3, we can see very small difference between the proposed method and conventional chirp scaling method on the image quality measurements, i.e., spatial resolution, PSLR and ISLR.

The second experiment utilized a real TerraSAR image as distributed targets scene containing three ships in the ocean (see Fig. 6). The imaging result according to the conventional DPCA SAR is shown in Fig. 7. The imaging results by the proposed spaceborne CS-HRWS SAR with different azimuth sampling rate (e.g., 50% and 25%) are shown in Fig. 8, which indicates that 25% sampling rate is still acceptable for ocean monitoring applications. Thus, the corresponding data rate is reduced to as low as 362 Mbps.

7. CONCLUSIONS

Spaceborne azimuth DPCA technique is an effective approach for implementation of HRWS SAR imaging. However, the multi-channel receivers in DPCA lead to huge volume data, which challenges both on-board storage and downlink subsystem of the SAR satellite. The conventional applications of CS in SAR imaging can utilize far fewer samples of echo signals to produce SAR images, but it also comes along the common drawback that recovery performances is under investigation.

In addition, direct application of CS in multiple channel SAR system will lead to spectrum aliasing caused by non-uniform sampling. To solve such problems, azimuth multiple channels based SAR mode, a novel scheme for each channel data sparse sampling and processing based on CS is proposed. The proposed method can not only reducing the heavy burden resulting from large volume of data acquisition and storage, but also it is possible to utilize far fewer samples in azimuth direction to produce high-quality images. It can be applied to spaceborne azimuth DPCA SAR systems, without changing its acquisition scheme. It only needs modify the on-board data handling subsystem, for dealing with the computation loads resulting from time domain sparse processing and frequency domain sparse representation procedures. The effectiveness of the proposed method has been proved by simulation and evaluation results.

ACKNOWLEDGMENT

The work described in the paper was supported in part by the National Key Basic Research Program Project under Grant 2010CB731902, and in part by National Natural Science Foundation of China under Grant No. 61132006.

REFERENCES

1. Zhang, M., Y. W. Zhao, H. Chen, and W.-Q. Jiang, "SAR imaging simulation for composite model of ship on dynamic ocean scene," *Progress In Electromagnetics Research*, Vol. 113, 395–412, 2011.
2. An, D. X., Z.-M. Zhou, X.-T. Huang, and T. Jin, "A novel imaging approach for high resolution squinted spotlight SAR based on the deramping-based technique and azimuth NLCS principle," *Progress In Electromagnetics Research*, Vol. 123, 485–508, 2012.
3. Nie, X., D.-Y. Zhu, and Z.-D. Zhu, "Application of synthetic bandwidth approach in SAR polar format algorithm using

the deramp technique," *Progress In Electromagnetics Research*, Vol. 80, 447–460, 2008.

4. Wang, Y., J. Li, J. Chen, H. Xu, and B. Sun, "A novel non-interpolation polar format algorithm using non-lineal flight trajectories and auto-adaptive PRF technique," *Progress In Electromagnetics Research*, Vol. 122, 155–173, 2012.
5. Xu, W., P. Huang, and Y.-K. Deng, "MIMO-tops mode for high-resolution ultra-wide-swath full polarimetric imaging," *Progress In Electromagnetics Research*, Vol. 121, 19–37, 2011.
6. Gerhard, K., G. Nicolas, and M. Alberto, "Unambiguous SAR signal reconstruction from nonuniform displaced phase center sampling," *IEEE Geoscience and Remote Sensing Letters*, Vol. 1, No. 4, 260–264, Oct. 2004.
7. Xu, W., P. Huang, and Y.-K. Deng, "Multi-channel SPCMB-tops SAR for high resolution wide-swath imaging," *Progress In Electromagnetics Research*, Vol. 116, 533–551, 2011.
8. Ma, L., Z.-F. Li, and G. Liao, "System error analysis and calibration methods for multi-channel SAR," *Progress In Electromagnetics Research*, Vol. 112, 309–327, 2011.
9. Guo, D., H. Xu, and J. Li, "Extended wavenumber domain algorithm for highly squinted sliding spotlight SAR data processing," *Progress In Electromagnetics Research*, Vol. 114, 17–32, 2011.
10. Donoho, D., "Compressed sensing," *IEEE Trans. on Inf. Theory*, Vol. 52, No. 4, 1289–1306, Apr. 2006.
11. Baraniuk, R., "Compressive sensing," *IEEE Signal Process.*, Vol. 24, No. 4, 118–121, Jul. 2004.
12. Candes, E., J. Romberg, and T. Tao, "Robust uncertainty principles: Exact signal reconstruction from highly incomplete frequency information," *IEEE Trans. on Inf. Theory*, Vol. 52, No. 2, 489–509, Feb. 2006.
13. Gurbuz, A. G., J. H. McClellan, and W. R. Scott, "A compressive sensing data acquisition and imaging method for stepped frequency GPRs," *IEEE Transitions on Signal Processing*, Vol. 57, No. 7, 2640–2650, Jul. 2009.
14. Herman, M. A. and T. Strohmer, "High-resolution radar via compressed sensing," *IEEE Transactions on Signal Processing*, Vol. 57, No. 6, 2275–2284, Jun. 2009.
15. Wei, S.-J., X.-L. Zhang, J. Shi, and G. Xiang, "Sparse reconstruction for SAR imaging based on compressed sensing," *Progress In Electromagnetics Research*, Vol. 109, 63–81, 2010.

16. Wei, S.-J., X.-L. Zhang, and J. Shi, "Linear array SAR imaging via compressed sensing," *Progress In Electromagnetics Research*, Vol. 117, 299–319, 2011.
17. Baraniuk, R. and P. Steeghs, "Compressive radar imaging," *Proc. IEEE Radar Conf.*, 128–133, Boston, MA, Apr. 2007.
18. Varshney, K. R., M. Cetin, and J. W. Fisher, "Sparse representation in structured dictionaries with application to synthetic aperture radar". *IEEE Transactions on Signal Processing*, Vol. 56, 3548–3561, 2008.
19. Patel, V. M., G. R. Easley, and D. M. Healy, "Compressed synthetic aperture radar," *IEEE Journal of Selected Topics in Signal Processing*, Vol. 4, No. 2, 224–254, Apr. 2010.
20. Tropp, J. A. and A. C. Gilbert, "Signal recovery from random measurements via orthogonal matching pursuit," *IEEE Trans. on Inf. Theory*, Vol. 53, No. 12, 4655–4666, Dec. 2007.
21. Ni, Z. W., M. Zhang, J. Li, and Q. Wang, "Image compressed sensing based on data-driven adaptive redundant dictionaries," *Progress In Electromagnetics Research M*, Vol. 22, 73–89, 2012.
22. Cai, J.-L., C.-M. Tong, W.-J. Zhong, and W.-J. Ji, "3D imaging method for stepped frequency ground penetrating radar based on compressive sensing," *Progress In Electromagnetics Research M*, Vol. 23, 153–165, 2012.
23. Wang, G. H. and Y.-L. Lu, "Sparse frequency waveform design for MIMO radar," *Progress In Electromagnetics Research B*, Vol. 20, 19–32, 2010.